Magnetization, neutron-, and resonant x-ray-diffraction studies of $U_{0.85}Th_{0.15}Sb$

J. A. Paixão* and G. H. Lander

Commission of the European Communities, Joint Research Centre, Institute for Transuranium Elements, Postfach 2340,
D-7500 Karlsruhe, Federal Republic of Germany

C. C. Tang and W. G. Stirling

Physics Department, School of Physical Science and Engineering, University of Keele, Keele, Staffordshire ST5 5BG, United Kingdom

A. Blaise and P. Burlet

Centre d'Etudes Nucléaires, 85X, 38041 Grenoble, France

P. J. Brown

Institute Laue-Langevin, Boîte Postale 156, 38042 Grenoble CEDEX 9, France

O. Vogt

Laboratorium für Festkorperphysik, Eidgenössische Technische Hochschule Zürich, CH-8093 Zürich, Switzerland

The magnetic phase diagram of USb-ThSb solid solutions was reported 10 years ago, but we have reexamined single crystals of (nominal) $U_{0.85}Th_{0.15}Sb$ following some unusual results found using synchrotron x-ray techniques. We show by magnetization that the material becomes antiferromagnetic at $T_N \sim 190$ K, but that a strong ferromagnetic moment develops below $T_C = 145$ K, and reaches $2.7\mu_B$ per U atom in high fields and at low temperature. Neutron diffraction (in zero field) on the same (and another) crystal indicates that the initial ordering near 190 K is incommensurate with $q_{inc} \sim 0.44$ reciprocal-lattice units (r.l.u.). At T_C the strong ferromagnetic component of $2.1\mu_B$ is seen, in addition to components $q = \frac{1}{4}$ and $\frac{3}{4}$ r.l.u. The ratio of the intensities of these antiferromagnetic components is close to that expected for a square-wave modulation $(4+, 4-)$. The q_{inc} component disappears near T_C but a small $q = \frac{1}{2}$-r.l.u. component is left. The presence of this component, also found in the same ratio in a second crystal, implies that a square-wave arrangement cannot be present. Various models to explain these results are presented. Synchrotron x-ray scattering has also been used to examine the same crystal. At the M_{IV} resonance (3.73 keV) the magnetic scattering is easily observable. The magnetic diffraction pattern corresponds to that determined with neutrons, except that the $q = \frac{1}{2}$ component is larger in the x-ray pattern. The difference between the neutron and x-ray results suggests that the near-surface magnetic structure as probed by x rays (~ 0.5-μm penetration) is different from that in the bulk, and that the magnetic structure in the near-surface region may be closer to a square wave. X-rays of 8-keV energy have also been used to examine the (100) d space as a function of temperature. An interesting broadening of the transverse, but not longitudinal, width is seen at T_C. We ascribe these changes to finite-size effects of the magnetic domains. We conclude by discussing the additional advantages of using synchrotron x-rays in studies of actinide magnetic structures.

I. INTRODUCTION

We have performed a series of synchrotron x-ray experiments on antiferromagnetic uranium compounds with the incident energy tuned near their M absorption edges. McWhan et al.[1] showed that at these absorption edges a very strong enhancement of the *magnetic* x-ray scattering amplitude occurs, giving rise to readily observable resonant magnetic x-ray scattering. Our previous work[2] was concerned with the resonance aspect (i.e., energy dependence) of this phenomenon; in all cases the materials had magnetic structures that were established many years ago by neutron diffraction. One of the samples (all single crystal in form) examined in Ref. 2 was a pseudobinary $U_{0.85}Th_{0.15}Sb$. In this case we thought also that we knew its magnetic structure, and the main purpose was to search for any effect at the Th resonance. None was found. In performing the x-ray synchrotron experiments, however, we became aware that the observed diffraction pattern did not conform to the published magnetic structure. The results, in fact, were so puzzling that we then instigated a study of the *same crystal* with the more conventional techniques of magnetization and neutron diffraction. This paper reports our findings from all three techniques, magnetization, neutron-, and synchrotron x-ray diffraction. We shall report the results in this order for clarity, even though the x-ray scattering experiments were done first.

The plan of the paper is as follows: The background on the magnetic structure is given in Sec. II, the magnetization in Sec. III, the neutron measurements in Sec. IV, the magnetic structure as seen by these two techniques in

Sec. V, the x-ray experiments in Sec. VI, and a summary in Sec. VII.

II. MAGNETIC STRUCTURE: PREVIOUS RESULTS

The magnetic structure[3] of USb (NaCl crystal with $a = 6.191$ Å) is type I with $T_N \sim 212$ K. In this structure, sheets of (001) planes are coupled together in the simple alternating sequence $+ - + -$. In neutron-diffraction studies there are no reflections of the form (100), (010), or (001) in the magnetic pattern. The intensities in magnetic neutron diffraction[4] are governed by both the magnetic structure factor and the magnetic interaction vector $Q_\perp$. The latter term is proportional to $\sin^2\alpha$, where α is the angle between the moment direction μ and the scattering vector Q. Thus, the absence of magnetic reflections along the principal cube directions $\{h00\}$ would normally imply that the moments were parallel to a cubic direction (and hence $\alpha = 0$). Such a model involves assuming three different domains, each domain consisting of a simple $+ - + -$ arrangement of moments with the moments parallel to the propagation direction q. This is called a single-q structure, and for USb the magnitude of q is 1. Another, more complex, model may be obtained by assuming that the three components of the modulation, each along a particular cube direction, exist *simultaneously* within certain crystallite. This is the so-called 3q structure.[5] The diffraction patterns of all multi-q structures are *identical,* so that the neutron-diffraction pattern alone cannot be used to decide which one is correct.

One way to distinguish among multi-q structures is to apply an external perturbation such as a uniaxial stress or magnetic field. This has been done for USb and firmly establishes[6] that the structure is 3q. There are two important consequences of a 3q structure: (i) the moment direction alternates throughout the crystal among all possible $\langle 111 \rangle$ directions, and (ii) the overall symmetry of the magnetic structure remains *cubic.*

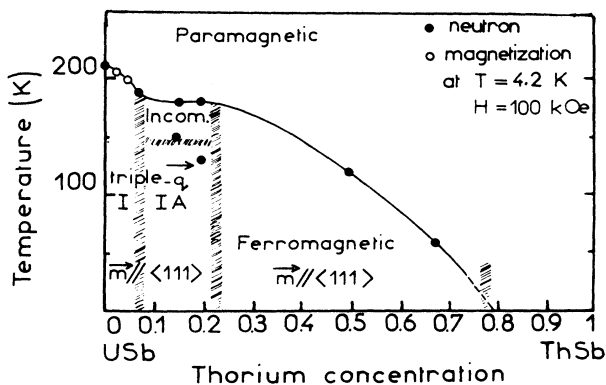We show in Fig. 1 the phase diagram of the

FIG. 1. Magnetic phase diagram of the (U,Th)Sb solid solution as published by Rossat-Mignod *et al.* (1982). The phases I and IA are antiferromagnetic with components $+ -$, and $+ + - -$, respectively. Incom. refers to an incommensurate structure. The vertical hatched marks correspond to regions in which more than one phase was found.

$U_{1-x}Th_xSb$ solid solution.[5,7] Doping tetravalent Th^{4+} into trivalent USb adds one electron per Th atom to the conduction band and the resulting change in the Ruderman-Kittel-Kasuya-Yosida interaction tends to drive the system ferromagnetic.[8] Thus, as x increases q tends to zero, reaching that value at $x \sim 0.22$, according to Fig. 1. For $x < 0.25$ other structures are formed with $0 < q < 1$. These correspond to structures with longer repeat unit cells. The best known of these is the type-IA structure, with $q = 0.5$, and a repeat unit cell consisting of a stacking $+ + - -$, etc. This appears in the $(U_{1-x}Th_xSb)$ phase diagram for $x = 0.07$. An incommensurate phase with $q \sim 0.515$ appears for $x = 0.15$ at T_N.

The tendency for q to decrease with increasing electron concentration has also been observed in many other systems, e.g., USb-UTe,[9] UP-US,[10,11] and UAs-USe,[12] as has the development of long-range antiferromagnetic structures. Another common feature is that for a given composition more than one phase is often found at a single temperature. This is true for experiments on both polycrystalline and single-crystal samples, and is usually ascribed to a variation in x across a given sample. An analysis of the NMR linewidths in a similar system[13] was interpreted in terms of a variation of dopant concentration of about 5% across a macroscopic sample. No direct evidence for non-square-wave modulations or structures containing "paramagnetic planes," as found in Ce monopnictides,[14] has been presented for uranium compounds at low temperature.

III. SAMPLE DETAILS AND MAGNETIZATION

The single crystals were grown at Eidgenössische Technische Hochschule (ETH), Zürich, using the mineralization technique.[15] New crystals were grown for the present work. The crystals have cleavage faces of (100) planes so that orienting them is simple. The crystals are mildly reactive with air so have to be kept in airtight containers. No special precautions were taken in our experiment to avoid short periods of contact with air, so that we assume that the (100) faces are coated with a UO_2 surface layer. *Magnetization, neutron-, and x-ray-diffraction experiments were performed on the same crystal* ($\sim 1 \times 1.5 \times 2$ mm). A larger crystal from the same batch was also used in the neutron experiment to examine the intensity of the higher harmonics.

Magnetization experiments were performed on a superconducting quantum interference device (SQUID) magnetometer (SHE design) at the Centre d'Etudes Nucleaires (CEN), Grenoble. The crystal was oriented with the applied field parallel to a $\langle 111 \rangle$ direction. Figure 2 shows the inverse susceptibility as a function of temperature in a field of 3 kOe. In the paramagnetic region ($T > 190$ K) the effective moment corresponds to $3.50(5)\mu_B$ per U ion. This is a value consistent with either a $5f^2$ or $5f^3$ configuration and, within experimental uncertainty, with the value of $3.6\mu_B$ found for USb.[16] It is clear from Fig. 2 that the material (at least in this applied field) is *ferromagnetic* for $T < 140$ K. This is inconsistent with a thorium concentration of $x = 0.15$ as shown in Fig. 1.[5,7]
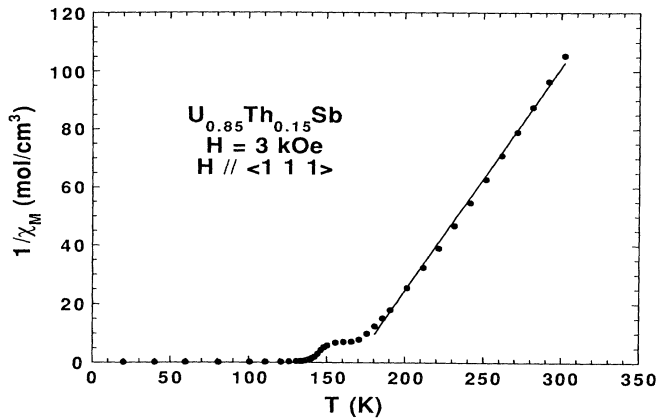
FIG. 2. Inverse susceptibility measured in an applied field of 3 kOe along a $\langle 111 \rangle$ axis as a function of temperature.

More details of the magnetic behavior are shown in Fig. 3. At low T the total moment is $2.3\mu_B$/formula unit (f.u.), i.e., $2.7\mu_B$/U, which is in excellent agreement with the total moment as deduced by Rossat-Mignod et al. However, Fig. 3(b) shows that another phase exists for low field over a region $145 < T < 190$ K. Using the infor-
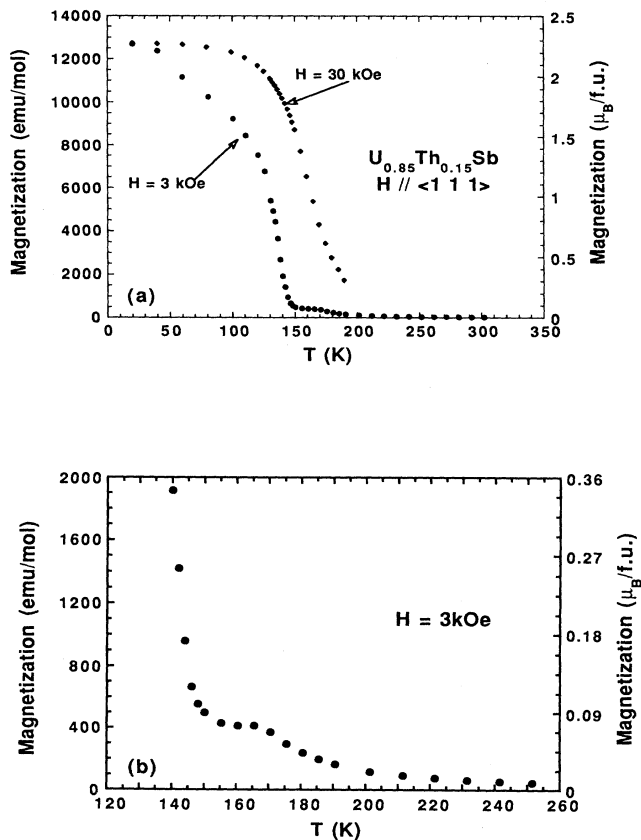

FIG. 3. Magnetization as a function of temperature. (a) Difference between magnetization at 3 and 30 kOe applied fields; (b) Details of magnetization at 3 kOe between 120 and 260 K.

mation in Fig. 1 we assume this is an antiferromagnetic state, which can be quenched by fields as high as 30 kOe.

IV. NEUTRON-DIFFRACTION EXPERIMENTS

The neutron experiments were initially performed at the D15 diffractometer at the Institut Laue-Langevin, Grenoble, but were later transferred to the Siloë reactor at the Centre d'Etudes Nucléaires, Grenoble. A double-axis instrument with an incident wavelength of 2.4 Å was used with appropriate pyrolytic graphite filters to remove higher-order contamination. The experimental resolution was 0.02 reciprocal-lattice units (r.l.u.) (~ 0.02 Å^{-1}). All experiments in the present study were performed in zero applied field. Figure 4 gives the results for the $q=0$, $\frac{1}{4}$, and $\frac{3}{4}$ components, all of which develop on cooling at 145 (3) K. Notice that the intensities for all three components are plotted on the same scale so that the largest effect is the increase in intensity at the (111) Bragg peak, i.e., the $q=0$ ferromagnetic component. This corresponds to $1.8\mu_B$/f.u. The presence of such a large ferromagnetic component along $\langle 111 \rangle$ implies a rhombohedral distortion at T_C (145 K). This distortion has not been observed directly in our experiments, but is a standard feature of all ferromagnetic UX materials.[17-19] Indirectly, we observe this macroscopic distortion through the accompanying relief of extinction (or a change of the mosaicity) in the crystal. As a result, strong Bragg reflections such as (200) increase in intensity below T_C. The (111) peak, on the other hand, with a weak intensity proportional to $|b_{U,Th} - b_{Sb}|^2$ is not sensitive to extinction effects and may be used to normalize the data and obtain the magnetic components in μ_B. In addition to a ferromagnetic component, we see components of $q=\frac{1}{4}$ and the third harmonic of this modulation. These may be recognized as components of a $4+,4-$ modulation, and have been studied recently by Jones et al.[20] in connection with the phase diagram of NpAs. Of course, in the latter material there is no ferromagnetic component, so the structure may be visualized rather simply. The situation is made even more difficult in this case by the observation of yet a fourth component at $q=\frac{1}{2}$. This is shown in Fig. 5(a). As we shall see, for $T > 145$ K, where the $q=0$, $\frac{1}{4}$, and $\frac{3}{4}$ components are absent, the structure is incommensurate and involved a single component near $q=0.5$. To give an overview of this behavior we show in Fig. 5(b) the total integrated intensity along the reciprocal lattice line from $0.45 < h < 0.55$ as a function of T.

Because of this unusual behavior of the magnetic components we have also examined a second crystal from the same batch, but ~ 10 times larger than the first crystal. The behavior of the two are very similar. Figure 5(c), for example, gives the q value of maximum intensity as a function of T of the incommensurate component. Crystal 1 is too small for us to measure this with neutrons below ~ 140 K. (All figures refer to crystal 1 unless otherwise stated).

V. MODELS FOR THE MAGNETIC ARRANGEMENT

We shall now discuss some of the possible moment configurations at low temperature ($T < 145$ K), when four components ($q = 0$, $\frac{1}{4}$, $\frac{1}{2}$, and $\frac{3}{4}$) are observed. In Table I we give the values in Bohr magnetons of the Fourier
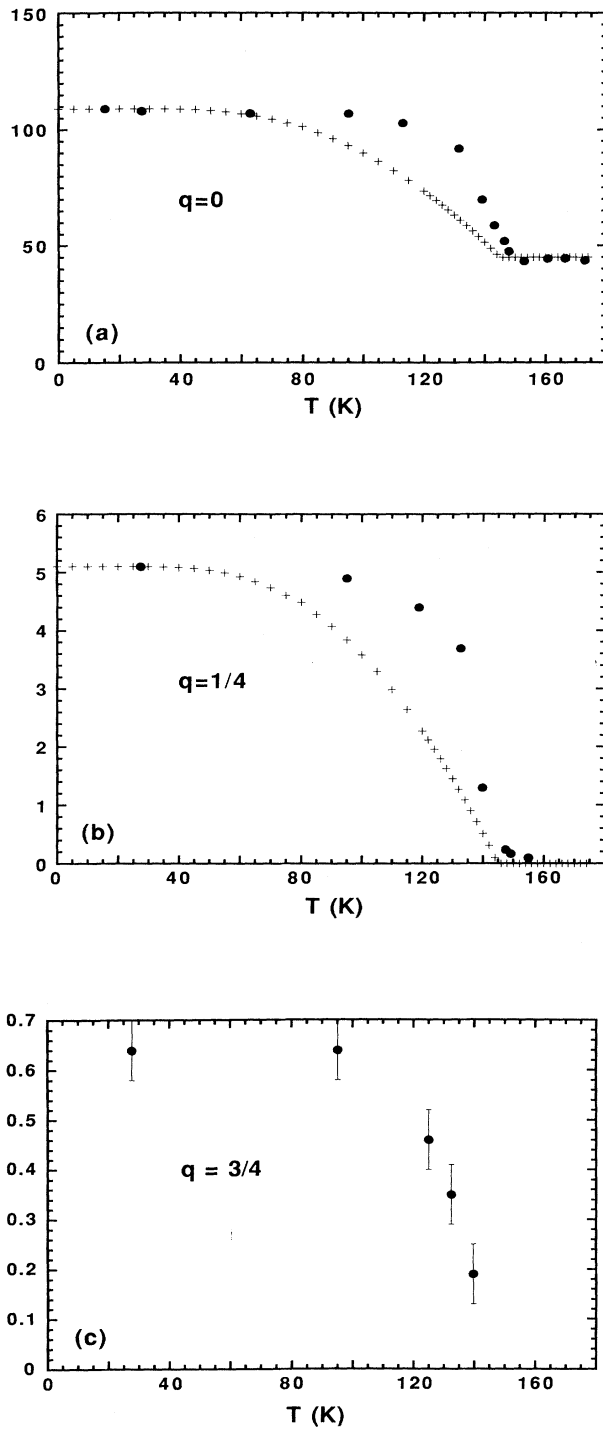

FIG. 4. Temperature dependence of the three major components to the magnetic modulation as measured by neutron diffraction (a) (111) nuclear reflection ($q = 0$) showing ferromagnetic contribution; (b) $q = \frac{1}{4}$ component; (c) $q = \frac{3}{4}$ component. Note that the *same* (arbitrary) scale is used throughout. The crosses give the squares of the Brillouin function ($S = \frac{1}{2}$) to emphasize the abrupt T dependence of the measured components. The T dependence of all three components if essentially the same.
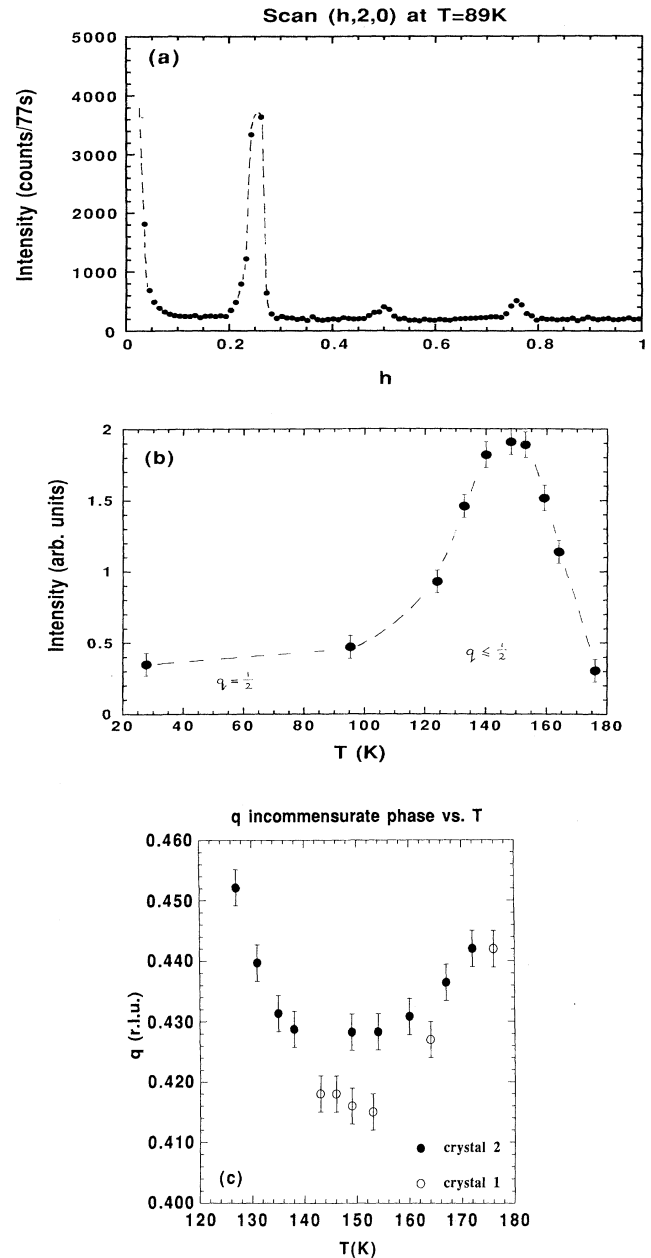
FIG. 5. (a) Experimental (neutron) scan at 89 K along the reciprocal lattice line $(h, 2, 0)$. The three components at $q = \frac{1}{4}$, $\frac{1}{2}$, and $\frac{3}{4}$ are shown. (b) Temperature dependence of the total intensity from $0.45 < h < 0.55$ in Fig. 5(a). The approximate division into $q = \frac{1}{2}$ and incommensurate q_{inc} is shown. (c) The wave vector of the incommensurate modulation q_{inc} as a function of temperature for the two crystals examined.

components as measured in the neutron experiment. We have also tabulated the ratio of the $q = \frac{1}{4}$ to $q = \frac{3}{4}$ Fourier components. For a square-wave $4+,4-$ structure the theoretical ratio is 2.41 and experimentally the ratio is close to this value. If we neglect for the moment the $q = \frac{1}{2}$ component, an initial model is to imagine a square wave $4+,4-$ modulation, but with a large ferromagnetic component. To achieve this we make the positive moments much larger than the negative ones in the $4+,4-$ modulation. Other methods of producing the observed harmonics may be imagined. In Table II we give the theoretical structure factors per atom (assuming 1 μ_B/atom) for the moment configurations shown. In our experiments there is no component at $q = 1$, so that this excludes more than half the models in Table II. Indeed, a comparison between Tables I and II shows that none of these models fits the experimental data.

It is clear from this comparison that we must reject a square-wave modulation, even at the lowest temperatures. One possible explanation could arise if we are prepared to accept that the sample consists of two distinct regions, one giving the $q = 0$, $\frac{1}{4}$, and $\frac{3}{4}$ components and the other the $q = \frac{1}{2}$ and q_{inc}. This argument cannot be rejected from the results of the magnetization and neutron-diffraction experiments. If that were the case, however, it is surely coincidental that the ratio of volumes of the two regions is the same in both crystals (Table I). We shall return later to this point, when we present the synchrotron studies.

The phases between these Fourier components cannot, of course, be determined from measuring diffracted intensities. The number of possible configurations is therefore infinite. However, if we assume that the system will try to minimize entropy, then the most likely configuration is that which minimizes the differences of each individual moment from the mean value. The sign of the moment is not considered. The parameters in such a model are the phases between the coefficients. The results of these "most probable configurations" are shown in Fig. 6. In the first simulation, Fig. 6(a), we show the "almost" square wave obtained by using all the coefficients from

TABLE I. Observed Fourier components (all in μ_B per U atom) for $U_{0.85}Th_{0.15}Sb$ at low temperature ($T < 100$ K). In the x-ray case we cannot observe a $q = 0$ component with our experimental arrangement, and the $q = \frac{1}{4}$ component has been *normalized* to the neutron value. We measure only relative intensities in the x-ray case, see text. Note that to combine the $q \neq 0$ components to project along the $\langle 111 \rangle$ direction, parallel to the $q = 0$ ferromagnetic component, they must be multiplied by $\sqrt{3}$.

| | Neutrons | | X rays |
	Crystal 1	Crystal 2	Crystal 1
$q = 0$ (F_0)	2.12(4)	2.15(4)	
$q = \frac{1}{4}$ ($F_{1/4}$)	0.55(2)	0.61(2)	[0.55]
$q = \frac{1}{2}$ ($F_{1/2}$)	0.14(1)	0.15(1)	0.27(3)
$q = \frac{3}{4}$ ($F_{3/4}$)	0.18(1)	0.20(1)	0.16(3)
$F_{1/4}/F_{3/4}$	3.1(2)	3.0(2)	3.5(3)

TABLE II. Magnetic structure factors deduced for the various harmonics as a function of the various *square-wave* modulations shown in the first column. In each case the values are in μ_B per atom, and $1\mu_B$/atom is used in the model. The last two rows correspond to the only possible models with paramagnetic planes (see text) that give zero amplitude at $q = 1$. To compare with the observed intensities in Table I it is important to note that for all components $q > 0$ one should divide the numbers in Table II by $\sqrt{3}$. This is because the $q > 0$ components are observed along $\langle 100 \rangle$, whereas the actual modulation is along $\langle 111 \rangle$, the body diagonal of the unit cell.

Spin configuration	$q = 0$	$q = \frac{1}{4}$	$q = \frac{1}{2}$	$q = \frac{3}{4}$	$q = 1$
$+ - + - + - + -$	0	0	0	0	1
$+ + - - + + - -$	0	0	0.707	0	0
$+ + + + - - - -$	0	0.653	0	0.271	0
$+ + + + + - - -$	0.25	0.604	0.25	0.104	0.25
$+ + + + - + - -$	0.25	0.433	0.25	0.433	0.25
$+ + + - + - + -$	0.25	0.25	0.25	0.25	0.75
$+ + + - + + - -$	0.25	0.25	0.559	0.25	0.25
$+ + + + + + - -$	0.5	0.462	0.354	0.191	0
$+ + + + + - + -$	0.5	0.354	0	0.354	0.5
$+ + + + - + + -$	0.5	0.191	0.354	0.462	0
$+ + + - + + + -$	0.5	0	0.5	0	0.5
$+ + + + + + + -$	0.75	0.25	0.25	0.25	0.25
$+ + + + + + 00$	0.75	0.231	0.177	0.096	0
$+ + + + 0 + + 0$	0.75	0.096	0.177	0.231	0

the neutron experiments (crystal 1), except the $F_{1/2}$ coefficient. The configuration outlined with a dash line has $F_{3/4} = F_{1/4}/2.41$. In Fig. 6(b) we then add the $F_{1/2}$ term; although this is small, there is an appreciable change in the configuration. Finally, in Fig. 6(c) we show a possible configuration derived from the x-ray amplitudes, which we shall discuss later.

We should emphasize the unusual nature of this $T = 0$ K magnetic structure. In a number of materials [e.g., $CeAl_2$,[21] NpP,[22] and $NpRu_2Si_2$ (Ref. 23)] the low-temperature magnetic structure is known not to be a square wave. However, in all these cases at most two magnetic components are observed in the diffraction pattern, and they cannot be combined together to form a square-wave configuration. Another example is $USb_{0.8}Te_{0.2}$, which exhibits many properties[24] similar to the present compound, and has ferromagnetic and incommensurate components existing together in the temperature range from 150 to 170 K. However, when many components are found in the diffraction pattern there is a tendency to assume that either they can be combined together with the right choice of a phase angles to make a square wave, or that some of them arise from physically different regions of the same sample.

The original work on the USb-ThSb solid solutions[7] determined that 3q antiferromagnetic structures existed for small Th doping. These measurements were performed in a large applied field. We have not repeated such investigations; instead, as shown below, we have independent evidence to confirm the 3q nature of the antiferromagnetic components.
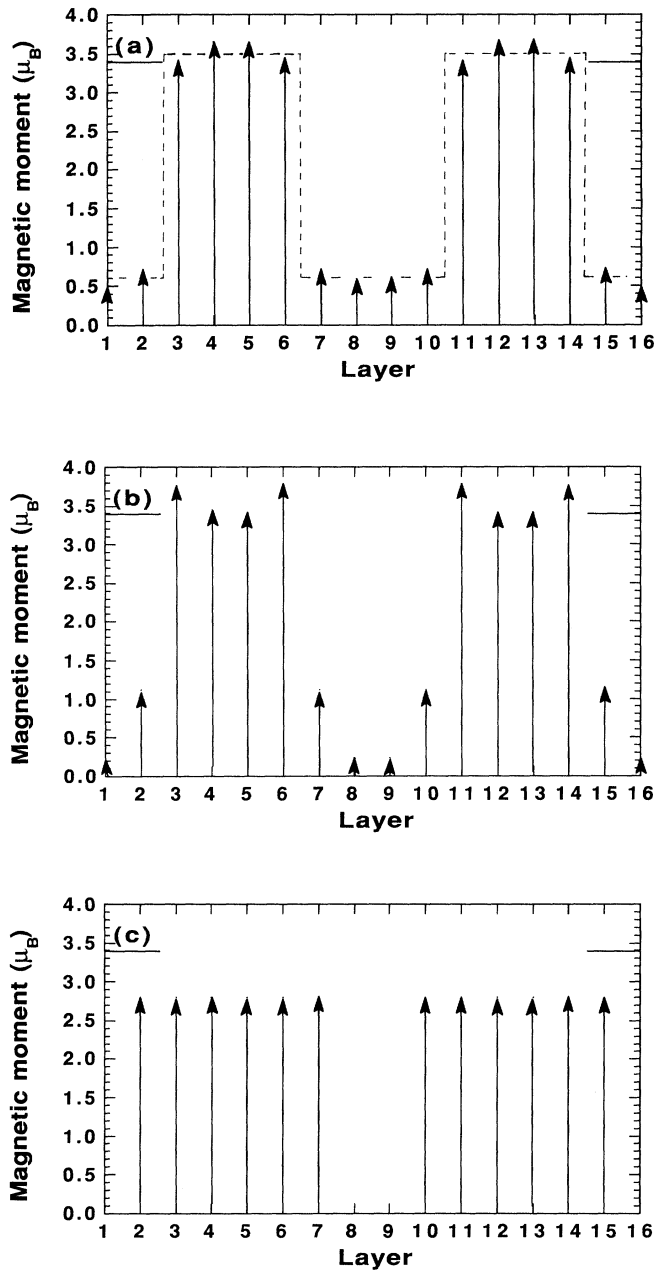
FIG. 6. Models of the magnetic configuration at low temperature in $U_{0.85}Th_{0.15}Sb$. The horizontal line at $3.4\mu_B$ is the maximum possible moment gJ for a U f^3 state. In each case two complete magnetic repeat units are shown. Recall that the modulation is longitudinal, but is shown as transverse for simplicity. (a) Result of combining observed neutron F_0, $F_{1/4}$, and $F_{3/4}$ components and minimizing the entropy (see text). The square-wave modulation (with a ratio of 2.41 between $F_{1/4}$ and $F_{3/4}$ is shown as a broken line). (b) Result of adding the observed $F_{1/2}$ component, which results in a distortion of the square wave. (c) The 6+, 0, 0, structure. The x-ray intensities (Table I) suggest a structure that is more strongly modulated than that deduced from the neutron intensities. In particular, the models show that the moments on some sites are close to zero and approach the 6+, 0, 0, structure shown here. See also the structure factors listed in Table II.

VI. X-RAY INVESTIGATIONS

The x-ray experiments were performed on the X22C beam line at the National Synchrotron Light Source at Brookhaven National Laboratory. Full details of the beamline and experimental procedure have been given in our earlier paper[2] and will not be repeated here. For these studies we used an incident energy of 3.73 keV (3.324 Å), which corresponds to the energy of the M_{IV} absorption edge. As has been well established by studies of UAs,[1] URu_2Si_2,[25] and our own,[2] there is a very strong resonant enhancement of the weak x-ray intensity at this energy.

All scans were performed along a [001] direction, i.e., symmetrical Bragg diffraction from a flat face. In simple resonant electron dipole theory[26] the intensities from magnetic x-ray scattering are proportional to the quantity $(\hat{e}^* \times \hat{e}')\cdot\hat{\mu}$, where $\hat{e}$ and $\hat{e}'$ denote the incident and final polarization of the x-ray beam, respectively, and $\hat{\mu}$ represents the local quantization axis of the magnetic ion. Initially the synchrotron beam is almost completely plane polarized (σ), but the magnetic scattering causes a rotation $\sigma \rightarrow \pi$. The product $(\hat{e}^* \times \hat{e}')$ is parallel to the final wave vector k'. If the component of magnetization that is sensed with $(00l)$ type reflections is parallel to Q, the scattering vector $(Q=k-k')$, which we know to be the case from neutron studies, then the product $k'\cdot\hat{\mu}$ will be proportional to $\sin\theta$, where θ is the Bragg angle. This angle is always greater than zero in diffraction, and we therefore anticipate scattering along the $(00l)$ line representative of the magnetic modulation.

Figure 7 shows x-ray scans along the $(00l)$ direction at 220 and 15 K. The Néel temperature $T_N = 190\pm1$ K (see
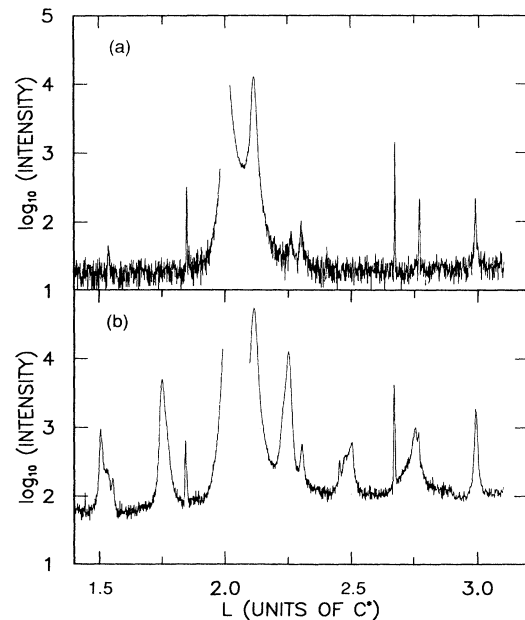

FIG.7. X-ray scans ($E = 3.37$ keV) along the [001] direction (a) at 220 K (above T_N) and (b) at 15 K. The intensity units are arbitrary, but the same in both (a) and (b).

Fig. 2 and below), so that the additional peaks in the 220-K pattern apart from the very strong $l=2$ charge peak must be due to nonmagnetic effects. Most of these peaks are relatively weak and can indeed be identified as higher-order peaks due to contamination of the incident beam, or as powder lines from the Cu sample holder, or from the Be windows. Thus the peak at (003) arises from $\lambda/2$ from the (006) and the peak at $l=2.667$ arises from $\lambda/3$ from (008). These peaks are effectively independent of temperature and need not be discussed further. The lower pattern (at 15 K) shows a number of new peaks, all of which are magnetic in origin. We have verified this not only be examining their T dependence (see below) but also their energy dependence. In the case of the strong reflections appearing at or near q vectors (measured from the charge peaks at $l=0,2,4$, etc.) of $\frac{1}{4}$, $\frac{1}{2}$, and $\frac{3}{4}$ we have found a characteristic rapid decrease in intensity as the energy is changed from 3.73 keV. Their symmetric energy dependence about the M_{IV} energy unambiguously identifies these peaks as arising from a modulation of the magnetic moments rather than from a lattice modulation.

A few qualitative remarks are in order before we analyze the x-ray pattern.

(1) Our x-ray measurements are insensitive to the ferromagnetic component. In principle, measurements of the ferromagnetic components is possible with x rays,[26] but we have not performed such type of experiment.

(2) The q-space resolution with x rays is about four times better in our configuration than with the neutron experiments discussed earlier.

(3) The x-ray magnetic satellite intensity from the same crystal for the U M_{IV} resonance is much stronger (in counts per second) than is possible with any neutron source.

(4) We cannot (yet) relate *resonant* intensities to the values of the magnetic moments.[26]

Thus the precise extent of the resonant enhancement of the nonresonant signal (this latter *is* related directly to the spin and orbital magnetization densities) depends on a number of factors, including matrix elements, core-hole life times, and the precise electronic ground state of the magnetic ion. Furthermore, from an experimental point of view, the data must be corrected for absorption, which is a difficult problem. Many of these aspects are discussed in our earlier work.[2] The result is that, whereas for a given compound the resonant enhancement is proportional to the magnetic moment (e.g., the T dependence of the moment may be accurately measured), the value of this proportionality constant is unknown.

We show scans taken in the high-temperature regime in Fig. 8. This and other experiments establish $T_N=190(3)$ K, in good agreement with Figs. 1–3. The growth of the incommensurate phase is also shown clearly in this figure, as well as its change with T and the growth of the $q=\frac{1}{2}$ component. Although the peaks in the incommensurate phase are asymmetric (this is also true in the neutron experiments) we have attempted to extract a value for q_{inc} by locating the centroid of the peak from the incommensurate phase. Figure 9 shows
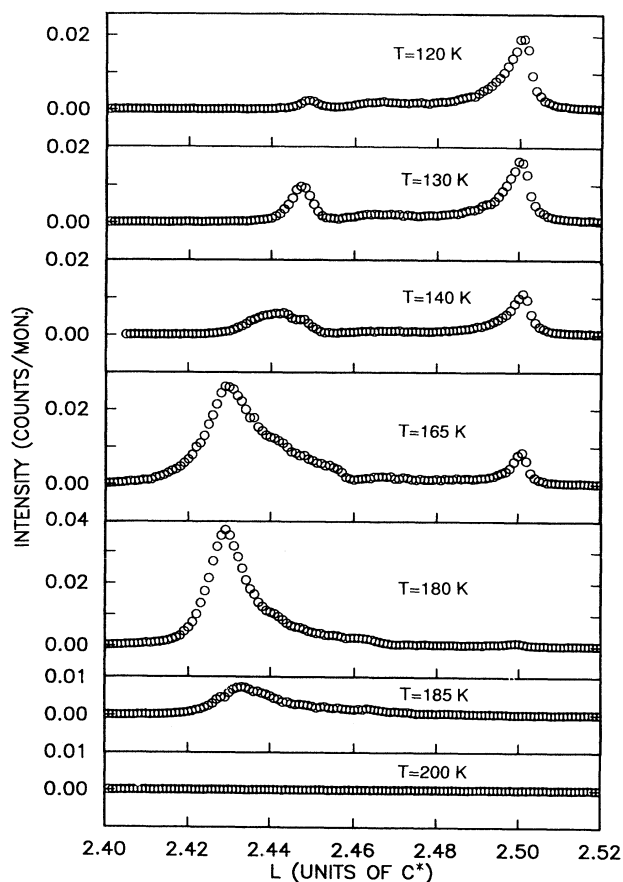

FIG. 8. Intensity ($E=3.73$ keV) as a function of temperature over the region $l=2.40-2.52$, corresponding to $q=0.40-0.52$.
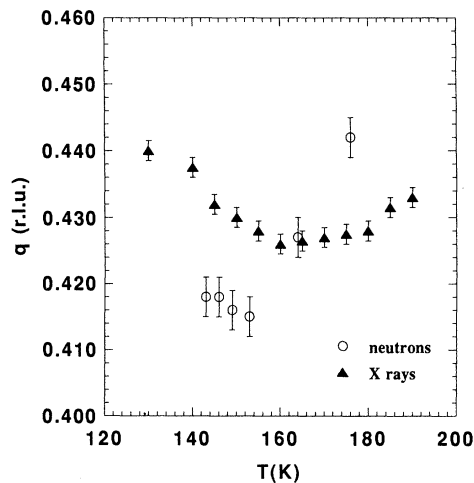

FIG. 9. Temperature dependence of incommensurate wavevector (q_{inc}) as measured by both neutrons and synchrotron x rays on crystal 1.

q_{inc} vs T from both neutrons [already presented in Fig. 5(c)] and x rays *on the same crystal*. There is a difference between these, which we consider to be significant and which we shall discuss further below.

We now turn to the T dependence of the $q = \frac{1}{4}$, $\frac{1}{2}$ and incommensurate components, which are shown in Fig. 10. In complete agreement with the neutron work (Fig. 4), we show the sudden appearance of the $q = \frac{1}{4}$ (and $q = \frac{3}{4}$ which is not shown in Fig. 10) below ~ 145 K. At low temperature we have integrated the intensities of the various satellites, corrected for the Lorentz factor, and the term $\mathbf{k}' \cdot \hat{\mu}$ discussed above in connection with the cross section. We stress that we cannot obtain absolute intensities, in Bohr magnetons, as possible in the neutron case. To discuss the relative magnitudes, we have *normalized* to the Fourier component of the $q = \frac{1}{4}$ satellite $F_{1/4}$, as measured by neutrons. These values are given in Table I. There are two points of interest. First, the ratio of $F_{1/4}$ to $F_{3/4}$ is the same within the experimental uncertainties as found by neutrons; second the $q = \frac{1}{2}$ component $F_{1/2}$ is considerably stronger in the x-ray case. (The *peak* intensities shown in Fig. 7 are not reliable, as this was obtained when the He pressure in the beam path[2] was varying. The integrated intensities as shown in Fig. 10 were obtained with an improved configuration and are reliable.) Clearly, the modulation is *different* as observed by x rays. Since the absorption of x rays on resonance is of order 25 000 cm^{-1} the penetration of these x rays is about 0.4 μm (4000 Å), whereas the neutrons are a *bulk* probe. The x rays therefore are probing the "near-surface" behavior. It is perhaps not surprising that with such a complex magnetic structure, changes occur near the surface; particularly in view of the well-known reactivity of these samples and the probable oxide overlayer.

To model the magnetic structure of this near-surface region as probed by the x rays we have to increase the im-

portance of the $F_{1/2}$ component with respect to the other two antiferromagnetic components. The result, again assuming the same entropy argument as used earlier, is that the small moments in Fig. 6(b) are further reduced, giving a structure which is close to the 6+,0,0, structure illustrated in Fig. 6(c). It is interesting that this bears a close resemblance to the models including paramagnetic planes proposed for Ce monopnictides.[14]

All the magnetic peaks are wider than the lattice peaks in the longitudinal direction. This means that the spatial coherence of the magnetic structure along the propagating direction is finite. Similar remarks were made in the case of the x-ray study of the near-surface structure of URu$_2$Si$_2$.[24] To obtain a measure of the magnetic correlations we assume that the resolution is given by the lattice peaks. We then deconvolute the observed magnetic peaks with this resolution function to obtain an intrinsic width. Following diffraction theory, and assuming that the broadening function is a Lorentzian, we may equate the mean correlation length ξ in real space to $1/\kappa$, where 2κ is the full width at half maximum (FWHM) of the Lorentzian function in reciprocal space. For the $q = \frac{1}{4}$ component we find $\xi \sim 300$ Å at 15 K, decreasing to ~ 100 Å at 140 K. The coherence length for the $q = \frac{3}{4}$ component is shorter at all temperatures than the $\frac{1}{4}$ component, ~ 120 Å at 15 K, and only ~ 80 Å at 140 K. The $q = \frac{1}{2}$ component is more complicated (see Fig. 8) because the peak shape is always asymmetric. Thus, a similar analysis has not been made.

A. X-ray: lattice behavior

We shall now turn our attention to the lattice behavior as a function of temperature. For these results the x-ray energy was increased to 8 keV and a Ge (111) analyzer was used to improve the resolution. The (100) d- space (d_{100}) is shown in Fig. 11(a) as a function of T. No
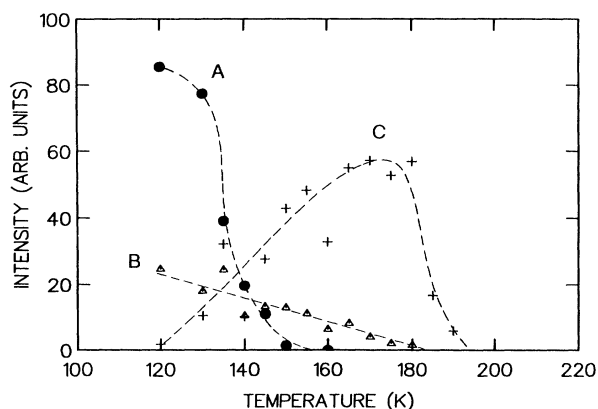

FIG. 10. Temperature dependence of the x-ray integrated intensity of the three major components of the magnetic structure. A the 4+,4− component giving peaks at $q = \frac{1}{4}$ and $\frac{3}{4}$. B is the 2+,2− component giving a peak at $q = \frac{1}{2}$, and C is the incommensurate component (in this case the sum of intensities from $q = 0.42$ to 0.46). The broken lines are guides to the eye.
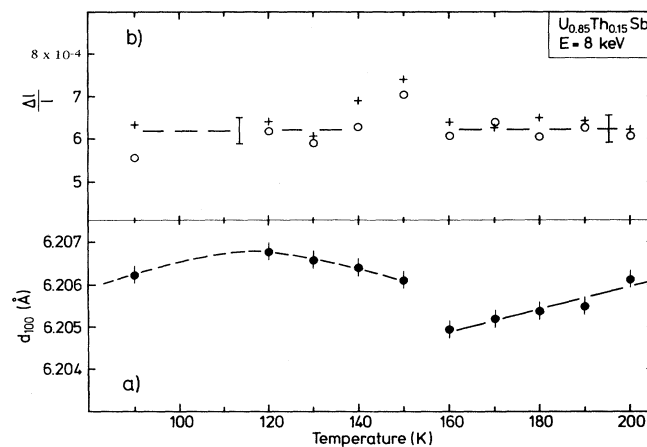

FIG. 11. Results from x-ray experiments obtained by examining the (002) and (004) lattice peaks [$E = 8$ keV and a Ge (111) analyzer]. (a) (100) d spacing, d_{100}. (b) Fractional longitudinal widths $\Delta l/l$. $\circ$ (002), + (004). The estimated error in these determinations is $\pm 0.3 \times 10^{-4}$, as shown by the error bars.

J. A. PAIXÃO *et al.*

anomaly is seen at T_N (190 K), but an expansion of the d space and an anomaly of $\Delta d/d = 2.3(2) \times 10^{-4}$ is observed at lower temperature. Referring to Figs. 4 and 10 it is clear that the expansion of d_{100} is associated with the appearance of the $q = 0$ and $q = \frac{1}{4}$ and $\frac{3}{4}$ components. We have also monitored both the longitudinal (Δl) and transverse $(\Delta \theta)$ width of the reflections (002) and (004). As shown in Fig. 11(b) the longitudinal width is *independent of temperature*, except for a possible small excursion near ~ 150 K. Both in the 3q state $145 < T < 190$ K and in the paramagnetic state $T > 190$ K this quantity d_{100} is the lattice parameter. Below 145 K in the ferromagnetic state d_{100} represents a d space at an angle of 54.7° to the unique $\langle 111 \rangle$ axis.

The experiments at 8 keV have considerable importance for understanding the *magnetic* behavior. One of the interesting questions here is whether the components $q = \frac{1}{2}$ and $q = \frac{1}{4}$ exist simultaneously in one crystal volume, or whether separate volumes contain either $q = \frac{1}{2}$ or $q = \frac{1}{4}$ components. The magnetic diffraction experiments with either neutrons or x rays are ambiguous on this point.

Assume that each crystallite in the sample belongs to one or other of the two phases A ($q = 0$, $\frac{1}{4}$, and $\frac{3}{4}$) or B ($q = \frac{1}{2}$), the choice depending on the local thorium concentration. This is the two-phase model. Since the magnetic moment is independent of Th concentration for $x < 0.30$ in $U_{1-x}Th_xSb$,[7] we expect comparable scattering intensities from similar volumes. However, the scattering from the $q = \frac{1}{2}$ component is weaker than that from the other components as seen in both the neutron- and x-ray-diffraction experiments. Within the two-phase model, this must mean that the volumes are unequal; in fact we can estimate $V_B/V_A \sim 0.25$ from the observed magnetic intensities (changing this ratio by $\pm 30\%$ does not affect the conclusions). The B component is already ordered at 170 K, so the d_{100} spacing for this B phase d_B should contract without any anomaly between 170 and 120 K. The A phase, on the other hand, orders at ~ 150 K. At this temperature there is a discontinuity [Fig. 11(a)] in the observed d_{100} of magnitude given by $\Delta d/d = 2.3(2) \times 10^{-4}$, which we assume is associated with the A phase. Thus, d_A is assumed to change at the ferromagnetic ordering temperature. The question is whether our experiments measuring the longitudinal width [Fig. 11(b)] would be sensitive to the existence of two phases having d_{100} spacings differing by a small quantity $\epsilon = 2(d_A - d_B)/(d_A + d_B)$, where the volume ratios of A and B are given by $V_B/V_A \sim 0.25$.

The experimental data are well represented by Lorentzians with full width at half maximum 2Γ. From Fig. 11(b) in which Δl is the full width at half maximum we see that $\Gamma(002) = 6.2 \times 10^{-4}$ r.l.u. (reciprocal lattice units) above 170 K. This value is kept fixed. We then performed *simulations* of the diffraction profile by superposing two profiles (their integrated intensities being in proportion to the volume ratio V_B/V_A) with steadily increasing separation of d_A and d_B, i.e., increasing ϵ. Two such resultant curves are shown in Fig. 12. Since Γ is fixed, it is convenient to consider the parameter ϵ/Γ.
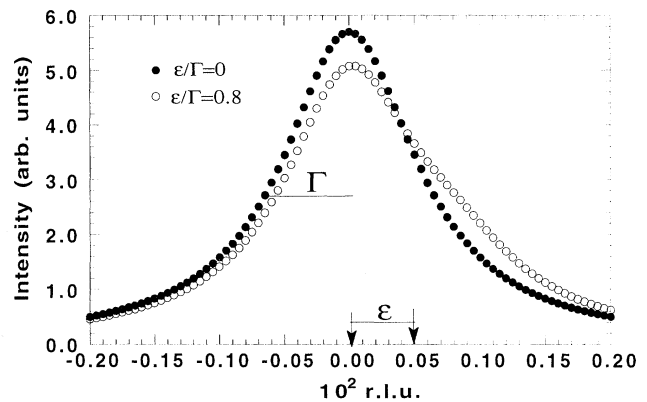

FIG. 12. Simulated profiles for the expected diffraction profiles in the two-phase model. Solid points are with $d_A = d_B$, i.e., $\epsilon = 0$, whereas the open points correspond to $\epsilon/\Gamma = 0.8$. See text for details.

The solid points have $\epsilon = 0$, i.e., there is no difference between d_A and d_B, whereas the open points have $\epsilon/\Gamma = 0.8$. In this latter case the peak shape is clearly deformed from a pure Lorentzian, and has a substantially larger half width at half maximum (HWHM) than the curve traced out by the solid points. By performing different simulations of this type, and measuring the HWHM, we can construct the expected variation as a function of ϵ/Γ. The result is shown in Fig. 13.

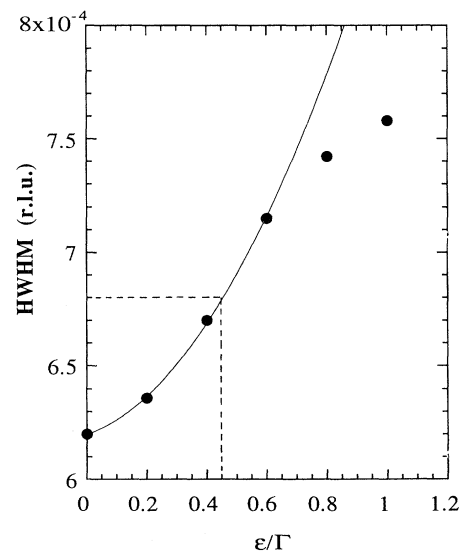The remarkable aspect of the longitudinal scans is that, apart from a possible small excursion near the transition

FIG. 13. Calculated variation of HWHM (half width at half maximum) as a function of ϵ/Γ, as defined in the text. The upper limit (dashed line) of a $\sim 10\%$ change in HWHM as measured in Fig. 11(b) is used to define the maximum possible separation of two discrete d spacings d_A and d_B in the proposed two-phase model.

at 150 K, the longitudinal widths [Fig. 11(b)] remain *constant* as a function of temperature. In particular Γ observed for $T < 150$ K is less than 6.8×10^{-4} r.l.u.; see Fig. 11(b). This corresponds to a maximum possible increase in the measured HWHM of $\sim 10\%$. For such an increase, the corresponding maximum value of ϵ / Γ may be obtained as 0.4 from Fig. 13. Thus $\epsilon_{max} < 0.4 \times \Gamma$, or $\epsilon_{max} < 2.5 \times 10^{-4}$. How does this relate to the observed differences between d_A and d_B? Figure 11(a) shows that the observed value of d_A changes by the fractional amount of $2.3(2) \times 10^{-4}$ at 150 K. Because the two-phase model assumes no relation between d_A and d_B, the difference between them would be expected to continue to increase down to 120 K, reaching a value of $\epsilon \sim 4 \times 10^{-4}$. But this value is greater than the value of ϵ_{max} derived above by analyzing the diffraction profiles.

The above argument appears to lead to the elimination of the two-phase model, and we conclude that all the magnetic components coexist in the same volume. This conclusion is based on an analysis of the *charge* scattering. It should be remembered, however, that in the near-surface region probed by our x-ray experiments, the lattice coherence length into the material ξ_L (as measured by the widths of the peaks) is very long, $\xi_L > 2000$ Å. On the other hand, as we have seen earlier, the magnetic coherence length ξ_M has a maximum of about 300 Å. Thus, over a distance where the lattice is essentially perfect, one could still imagine the possibility of a number of different magnetic domains, perhaps containing different ordering wave vectors. Some variation of the two-phase model could therefore still exist. This illustrates the difficulty in drawing conclusions about the near-surface region of the crystal when the magnetic ordering, even at low temperature, does not appear to be truly "long range."

We have also examined the diffraction profiles themselves, not simply the HWHM Γ. Some asymmetry is seen in the wings of the (004) at lower temperature, but not in those of (002). Because $\Delta l / l$ is the same for both of these, we would expect similar effects in both reflections even though the (004) is more sensitive to changes in d_{100} In brief, we believe these small changes in the l scans arise from coupling through the resolution function with transverse (rocking) scans. As discussed below, these exhibit very considerable broadening on passing through the ferromagnetic transition.

B. Lattice structure

The onset of the $q = 0$ ferromagnetic $\langle 111 \rangle$ component (Figs. 3 and 4) at 145 K will result in a rhombohedral distortion of the unit cell. We have not measured this distortion; it is too small to see in our neutron experiments and our x-ray experiments were confined to (00l) planes, which are not sensitive to a rhombohedral distortion. (However, see Sec. IV for indirect evidence of this macroscopic distortion in the neutron experiments.) We anticipate a value of $\sim 10^{-2}$ in terms of the strain[17-19] based on other ferromagnetic actinide NaCl-structure materials. On the other hand, we have emphasized that the antiferromagnetic components propagate along $\langle 100 \rangle$ and

couple to the ferromagnetic $\langle 111 \rangle$ component by virtue of the 3q nature of the antiferromagnetic (AF) structure. The rhombohedral angle would then change from 90° to $\sim 89.6°$. If the AF components were strictly single q then they would couple to the lattice causing a *tetragonal* distortion, which would be observable at (00l); see, for example, the work on NpAs which has the $4+,4-$ single-q structure.[22] Quite independent of the rhombohedral distortion, it is therefore of interest to examine the (00l) planes; the fact that Fig. 11(b) indicates no change in the longitudinal width is direct confirmation of the 3q nature of the AF component.

In addition to the longitudinal scans summarized in Fig. 11 we have also performed transverse (rocking) scans. A very substantial change occurs in the shape of the peaks, both in the FWHM and in the wings of the peaks. The integrated intensity of the peaks does not change as a function of temperature, but the width does. To illustrate this we show transverse scans taken with the high-resolution configuration (8 keV, Ge analyzer) for both the (002) and (004) Bragg reflections in Fig. 14 for temperatures above and below T_C. We emphasize that
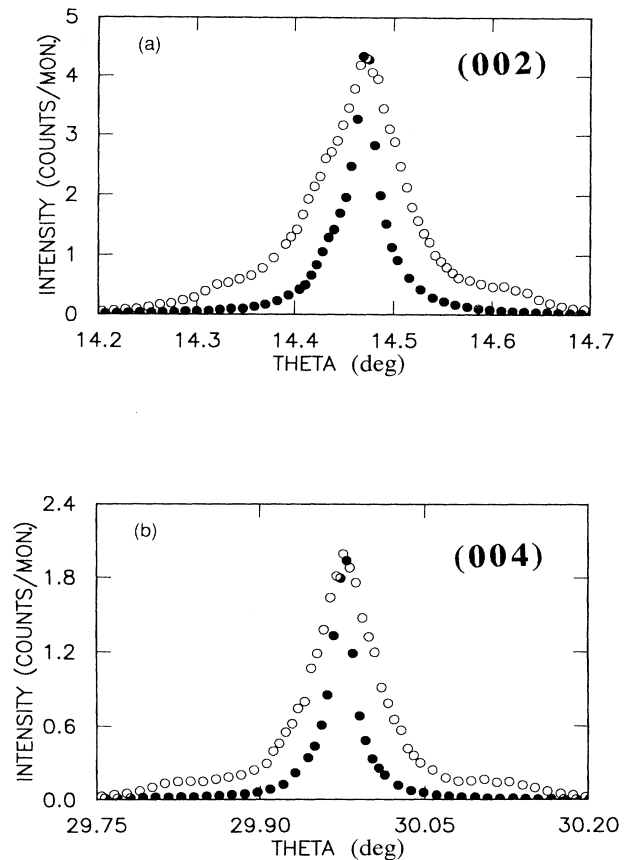

FIG. 14. Experimental x-ray rocking curves of (a) (002) and (b) (004) reflections at 180 and 120 K. The scale corresponds to the 180-K data (squares) in both cases. The 120-K data (open circles) has been normalized so that the peak coincides in height and position with the 180-K data. The integrated intensities do not change as a function of temperature.

the peaks have been normalized to give the same peak intensity; in reality the integrated intensity remains constant so that when the peak becomes broader the peak height decreases. The temperature dependence of the FWHM is shown in Fig. 15.

The rhombohedral distortion that occurs at ~ 145 K certainly introduces strain into the lattice, and the physical movement of the ferromagnetic domains could be observed as an increase in the mosaic distribution. This should give rise to an increase in the FWHM of the rocking curves (Fig. 15) that is independent of diffraction order. Such is not the case. It is not possible to measure such curves for the main magnetic component $(q = \frac{1}{4})$ because it disappears (Figs. 4 and 10) at 145 K, but we have examined the $q = \frac{1}{2}$ component as a function of temperature, and it remains constant with a width approximately the same as the (002) at low temperature (this must be done at 3.73 keV; in this configuration the resolution is not as good as in Fig. 15).

Changes in the shape of the diffraction profiles are, of course, phenomena that have been studied extensively in the past.[27] The two principal causes of changes in the diffraction profile are caused by changes in the volume of the diffracting region, or by changes in the relative orientation of the diffracting crystallites with respect to each other, or both. These effects can be separated by observing the diffraction profiles as a function of diffraction order. Changes in the orientation are independent of the diffraction order, whereas size effects depend on the momentum transfer, and should increase with increasing momentum transfer. Our results (Fig. 15) do not fit into either of these cases. Rather, the (002) is broadened by $\sim 50\%$ more than the (004) reflection. The combined evidence of these widths suggests a more subtle interpretation involving the volume of the ferromagnetic domains probed by the different Bragg geometries. Interpreting the broadening shown in Fig. 15 as a coherence length
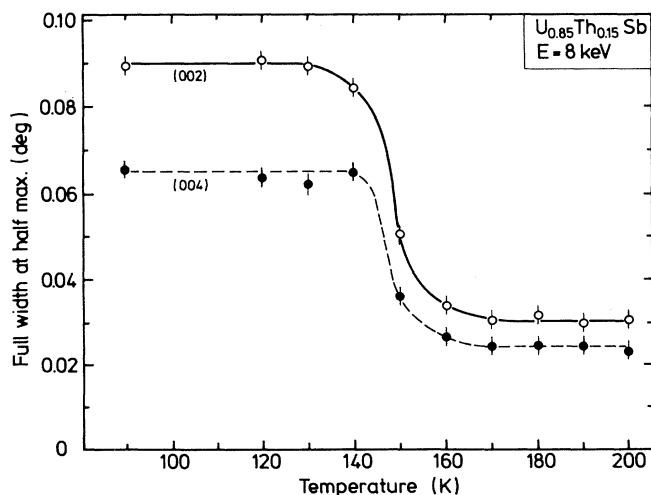

FIG. 15. Transverse widths of the (002) and (004) reflections as a function of temperature taken with the x-ray configuration as in Fig. 14.

(similar to the earlier discussion on the magnetic peaks) we find that for the (002) reflection $\xi \sim 1000$ Å and for the (004) reflection $\xi \sim 2000$ Å. Since the absorption of uranium at 8 keV is $\sim 12\,000$ cm^{-1} and the Bragg angles for (002) and (004) are 14.5° and 30°, respectively, the penetration depths for these two reflections are ~ 0.2 μm (2000 Å) for the (002) and about double this for the (004). Because the (002) reflection is thus more surface sensitive, we suggest that the ferromagnetic domains at the surface are smaller than those in the bulk, presumably due to the increased relaxation possible at the surface and/or due to the penetration of the oxide overlayer into the bulk of the crystal.

VII. SUMMARY

That the U-based solid solutions of NaCl type have complex magnetic structures is well established,[5] see, for example, the work of Kuznietz *et al.* on the UP-US solid solution.[10] We have *not* performed this study simply to show that the phase diagram of USb-ThSb has some additional complications. Clearly, our samples of nominally $x = 0.15$ are slightly different from those prepared previously. That is not the issue here; instead we illustrate in this study the additional information that is available with resonance magnetic scattering using synchrotron x rays. The complementarity of the three techniques employed is well illustrated. The important points are as follows:

(1) The magnetic structure, although dominated by a ferromagnetic component, is *not* a square wave at low temperature. Possible models are shown in Fig. 6. Interestingly, the near-surface structure (< 1 μm) as probed by x rays has a slightly different configuration.

(2) The high q-space resolution available with the x rays (resolution of 0.001 r.l.u. with 8-keV photons, see Fig. 11) has allowed two interesting points to be examined: (a) The simple idea that the components may exist in two distinctly different volumes can probably be eliminated, (b) in the low-temperature phase ($T < 145$ K) we find that the broadening of the lattice peaks suggests that the ferromagnetic domains near the surface are smaller than those in the bulk.

The two latter effects are both related to the near-surface region and its magnetic ordering. Since few studies of this sort have been reported, we are reluctant to draw firm conclusions. An earlier study[28] of the onset of long-range order in $Mn_{0.75}Zn_{0.25}F_2$ already drew attention to the startling differences that can be seen in the *same* crystal when using neutron and x-ray scattering, and we hope our work encourages other studies, especially those using the strong U resonance.

*On leave from Departamento de Fisica, Universidade de Coimbra, Portugal.

[1]D. B. McWhan, C. Vettier, E. D. Isaacs, G. E. Ice, P. Siddons, J. B. Hastings, C. Peters, and O. Vogt, Phys. Rev. B **42**, 6007 (1990).

[2]C. C. Tang, W. G. Stirling, G. H. Lander, D. Gibbs, W. Herzog, P. Carra, B. T. Thole, K. Mattenberger, and O. Vogt, Phys. Rev. B **46**, 5287 (1992).

[3]G. H. Lander, M. H. Mueller, D. M. Sparlin, and O. Vogt, Phys. Rev. B **14**, 5035 (1976).

[4]W. Marshall and S. W. Lovesey, *Theory of Thermal Neutron Scattering* (Oxford University Press, London, 1971), p. 152.

[5]For a complete review up to ~1983, see J. Rossat-Mignod, G. H. Lander, and P. Burlet, in *Handbook on the Physics and Chemistry of the Actinides*, edited by A. J. Freeman and G. H. Lander (North-Holland, Amsterdam, 1984), Vol. 1, p. 145.

[6]J. Rossat-Mignod, P. Burlet, S. Quezel, and O. Vogt, Physica B **102**, 237 (1980).

[7]J. Rossat-Mignod, P. Burlet, S. Quezel, O. Vogt, and H. Bartholin, in *Crystalline Electric Field Effects in f-Electron Magnetism*, edited by R. P. Guertin, W. Suski, and Z. Zolnierek (Plenum, New York, 1982), p. 501.

[8]See, for example, Q. G. Sheng and B. R. Cooper, J. Appl. Phys. **70**, 6083 (1991), and references therein.

[9]J. Rossat-Mignod, P. Burlet, O. Vogt, and G. H. Lander, J. Phys. C **12**, 1101 (1979).

[10]M. Kuznietz, P. Burlet, J. Rossat-Mignod, O. Vogt, and K. Mattenberger, Phys. Rev. B **35**, 7142 (1987); J. Magn. Magn. Matter. **63-64**, 165 (1987).

[11]O. Vogt and K. Mattenberg, J. Less Common Met. **133**, 53 (1987).

[12]M. Kuznietz, P. Burlet, J. Rossat-Mignod, and O. Vogt, J. Less Common Met. **121**, 217 (1987).

[13]M. Kuznietz, F. P. Campos, and Y. Baskin, J. Appl. Phys. **40**, 3621 (1969).

[14]J. Rossat-Mignod, J. M. Effantin, P. Burlet, T. Chattopadhyay, L. P. Regnault, H. Bartholin, C. Vettier, O. Vogt, D. Ravot, and J. C. Achart, J. Magn. Magn. Matter. **52**, 111 (1985).

[15]J. C. Spirlet and O. Vogt, in *Handbook on the Physics and Chemistry of the Actinides* (Ref. 5), p. 79.

[16]J. M. Fournier and R. Troc, in *Handbook on the Physics and Chemistry of the Actinides* (Ref. 5), Vol. 2, p. 29.

[17]G. H. Lander and M. H. Mueller, Phys. Rev. B **10**, 1994 (1974).

[18]T. Palewski, S. Weglowski, and R. Pajak, Physica B **86-88**, 111 (1977).

[19]F. Hulliger and O. Vogt, Physica B **102**, 316 (1980).

[20]D. L. Jones, W. G. Stirling, G. H. Lander, J. Rebizant, J. C. Spirlet, M. Alba, and O. Vogt, J. Phys. Condens. Matter **3**, 3551 (1991).

[21]B. Barbara, J. X. Boucherle, J. L. Buevoz, M. F. Rossignol, J. Schweizer, Solid State Commun. **24**, 481 (1977); E. M. Forgan, B. D. Rainford, S. L. Lee, J. S. Abell, and Y. Bi, J. Phys. C M **2**, 10 211 (1990).

[22]A. T. Aldred, B. D. Dunlap, A. R. Harvey, D. J. Lam, G. H. Lander, and M. H. Mueller, Phys. Rev. B **9**, 3766 (1974).

[23]P. Burlet, D. Bonnisseau, S. Quezel, J. Rossat-Mignod, J. C. Spirlet, J. Rebizant, and O. Vogt, J. Magn. Magn. Matter **63-64**, 151 (1987).

[24]P. Burlet, S. Quezel, J. Rossat-Mignod, G. H. Lander, and O. Vogt, J. Magn. Magn. Matter **14**, 309 (1979).

[25]E. D. Isaacs, D. B. McWhan, R. N. Kleinman, D. J. Bishop, G. E. Ice, P. Zschak, B. D. Gaulin, T. E. Mason, J. D. Garrett, and W. J. L. Buyers, Phys. Rev. Lett. **65**, 3185 (1990).

[26]M. Blume and D. Gibbs, Phys. Rev. Rev. B **37**, 1779 (1988); S. W. Lovesey, J. Phys. C **20**, 5625 (1987).

[27]B. D. Cullity, *Elements of X-Ray Diffraction* (Addison-Wesley, Reading, MA, 1978), p. 284; B. E. Warren, *X-Ray Diffraction* (Dover, New York, 1990), p. 264 *et seq.*

[28]J. P. Hill, T. R. Thurston, R. W. Erwin, M. J. Ramstead, and R. J. Birgeneau, Phys. Rev. Lett. **66**, 3281 (1991).